Electronic supplementary information

Cobalt nanoparticles shielded in N-doped carbon nanotubes for high areal capacity Li–S batteries

Lei Wei,[a] Wanlong Li,[a] Teng Zhao,*[a] Nanxiang Zhang,[a] Li Li,[ab] Feng Wu[ab] and Renjie Chen*[ab]

a. School of Materials Science & Engineering, Beijing Institute of Technology, Beijing 100081, China.

b. Collaborative Innovation Center of Electric Vehicles in Beijing, Beijing 100081, China.

* Corresponding author. Email: chenrj@bit.edu.cn (R. Chen); tz270@bit.edu.cn

1. Experimental section

1.1 Synthesis of the ZIF-67 sample.

All chemicals and solvents were of analytical grade and used without further purification. Typically, 4.65 mmol $Co(NO_3)_2 \cdot 6H_2O$ and 0.2 mol 2-methylimidazole ($C_4H_6N_2$, Aladdin, 98.0%) were dissolved in 9 mL and 60 mL deionized water, respectively. The two solutions were quickly mixed and stirred for 6 hours at room temperature. After centrifugation, the as-obtained precipitate was collected, washed with ethanol three times, and finally dried at 80 ℃ for 12 h, resulting in purple ZIF-67 nanocrystals.

1.2 Preparation of Co-NCNTs.

The as-prepared ZIF-67 material (0.5 g) was completely mixed with dicyandiamide (2.5 g), and the homogeneous mixture were put into a tube furnace and annealed at 550 ℃ for 3 h with a heating rate of 2 °C min^{-1} and further raised to 800 °C for 6 h at a ramp of 1 °C min^{-1} in Ar_2 atmosphere. After cooling down naturally, the Co-NCNTs products were obtained.

1.3 Fabrication of Co-NCNTs modified separator

The modified separator with Co-NCNTs were prepared by the doctor blade method. Co-NCNTs and polyvinylidene fluoride (PVDF) in a weight ratio of 8:1 were well-mixed and dispersed in N-methyl-2-pyrrolidinone (NMP) to form uniform slurry. Afterward, the slurry was coated onto one side of the Celgard 2400 polypropylene membrane. The Co-NCNTs modified separator was dried at 50 °C for 48 h and finally obtained with an areal mass loading of 0.23 mg cm^{-2}.

1.4 Preparation of the CNT/S cathode

The CNT/S cathode was prepared via a conventional melt-diffusion method. The commercial MWCNTs (10–20 nm in diameter, length >2 μm, purity >97%) were purchased from Shenzhen Nanotech Port Co., Ltd. First, the MWCNTs and sulfur powder with a weight ratio of 3:7 were thoroughly mixed and ball-milled for 1 h and sealed in a polytetrafluoroethylene container filled with Ar_2, followed by heating at 155 °C for 24 h. Then the obtained composite was mixed with Super P as conductive agent and PVDF as binder in NMP with a mass ratio of 7:2:1 to form a homogeneous slurry and casted onto the aluminum foil current collector. After dried at 50 ℃ for 24 h, the electrode was cut into circular disks with a diameter of 11mm. The areal mass loading of the active materials in the electrode was around 1.8, 2.7 and 4.3 mg cm^{-2}.

1.5 Materials characterizations

X-ray diffraction (XRD) patterns were recorded on a diffractometer (Rigaku Ultima IV-185, Japan) with a Cu Kα radiation (λ=0.154 nm). The detailed morphologies of the samples were observed using a field emission scanning electron microscope (FE-SEM, FEI Quanta 650, USA) and high resolution transmission electron microscopy (HR-TEM, JEM-2100F, Japan). The X-ray photoelectron spectroscopy (XPS) measurement was conducted on a XPS apparatus (Thermo ESCALAB 250Xi, USA) with a monochromatic Al Kα radiation. Thermogravimetric analysis (TGA, EXSTAR 6200, Japan) was carried out to determine the sulfur content under N_2 flow with a heating rate of 10 ˚C min^{-1}. TGA was also conducted to analyze the cobalt content in Co-NCNTs from room temperature to 800 ˚C with a heating rate of 10 ˚C min^{-1} in air.

1.6 Lithium polysulfide adsorption tests

The Li_2S_6 solution was prepared by adding Li_2S and S with a molar ratio of 1:5 into a mixture solvent of 1, 3-dioxolane (DOL) and 1, 2-dimethoxyethane (DME) (1:1 v/v) and violently stirred for 24 h at 50 °C. To conduct the lithium polysulfides adsorption tests, same mass MWCNT and Co-NCNT were soaked into 10 mL of 5 mM Li_2S_6 solution, respectively. Then it was rested for 12 h to evaluate the polysulfide absorption ability of different samples.

1.7 Assembly of Li_2S_6 symmetric cells and measurements

Two identical carbon cloth disks with a diameter of 11 mm were used as both working electrode and counter electrode in a symmetric cell configuration. To fabricate the electrodes, the 90 wt% host material (MWCNTs, Co-NCNTs) and 10 wt% PVDF were dispersed in NMP and coated onto carbon cloth with a mass loading of 2 mg cm^{-2}. The electrolyte was 1 M bis(trifluoromethane sulfonyl)imide (LiTFSI) and 0.2 M Li_2S_6 in DOL/DME mixture (1:1 v/v). The dosage of electrolyte was 40 μL in each cell. Cyclic voltammetry (CV) measurements of the symmetrical cells were performed at different scan rate (1, 2, and 3 mV s^{-1}) with the voltage ranging from −1.0 to 1.0 V. The electrochemical impedance spectroscopy (EIS) was measured using the CHI-660D (Shanghai, Chenhua) electrochemical workstation in a frequency range from 100 kHz to 0.01 Hz with an amplitude of 10 mV.

1.8 Electrochemical measurements

The CR2025 type coin cells were assembled in an argon filled glove box with CNT/S

composite as cathode, Li metal foil as anode and Co-NCNT or MWCNT modified Celgard 2400 polypropylene membrane as separator. The electrolyte was composed of 1 M LiTFSI in a mixture of DOL and DME (1:1 v/v) with 0.2 M $LiNO_3$ as additive. The amount of the electrolyte added into each coin cell was controlled with an electrolyte/sulfur ratio of 20 $uL_{(electrolyte)}$ $mg^{-1}_{(sulfur)}$. The cycling performance of the cells were galvanostatically tested on a multi-channel battery testing system (Land CT2001A, Wuhan, China) under different rates (1C= 1675 mA g^{-1}) in the voltage range of 1.7-2.8 V. The CV measurements were conducted on a CHI-660D electrochemical workstation at the same voltage window. The EIS was tested in the frequency range between 0.01 Hz and 100 KHz.

2. Supplementary Figures

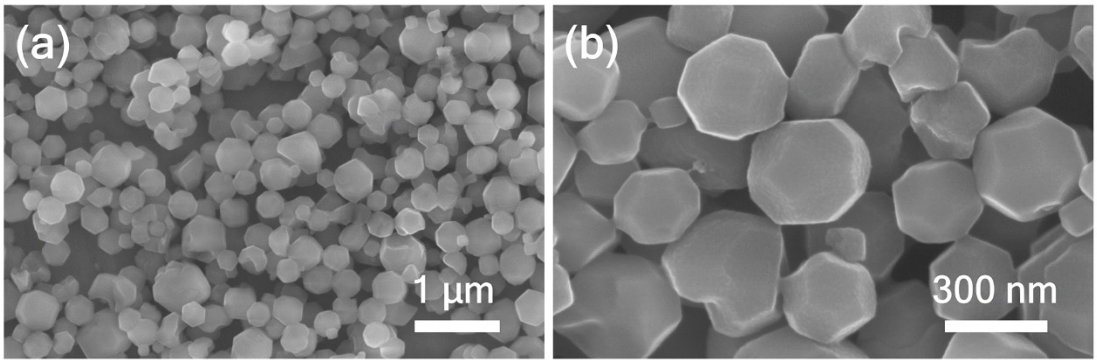

Fig. S1 SEM images of the precursor ZIF-67 (a) Low magnification. (b) High magnification.

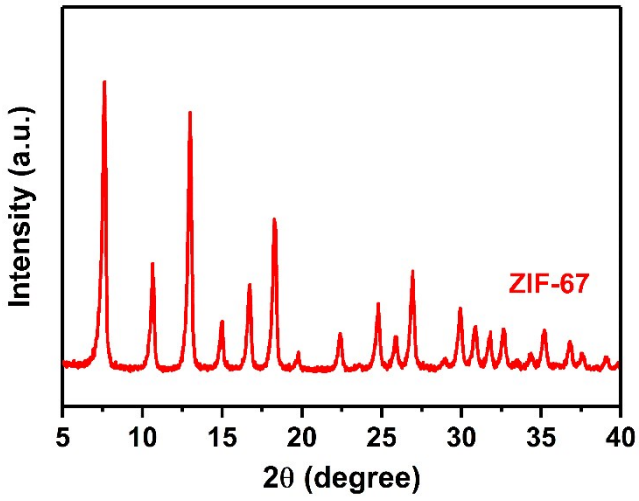

Fig. S2 X-ray diffraction pattern of the precursor ZIF-67.

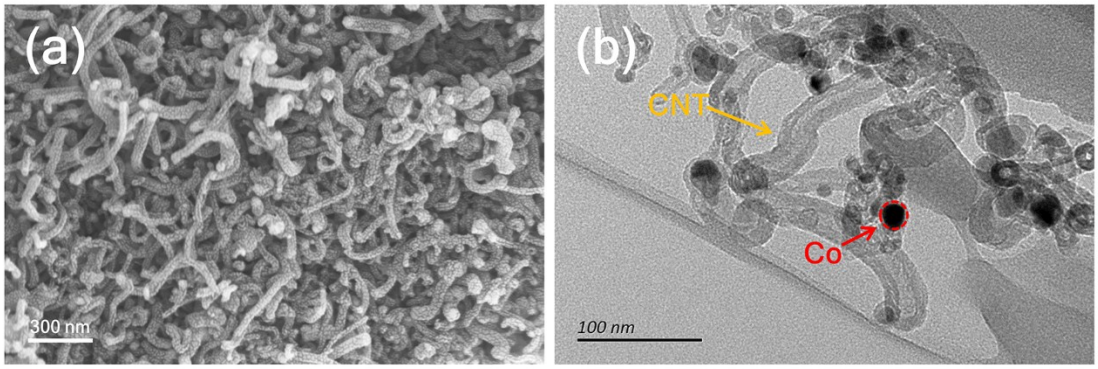

Fig. S3 SEM image (a) and TEM image (b) of Co-NCNTs.

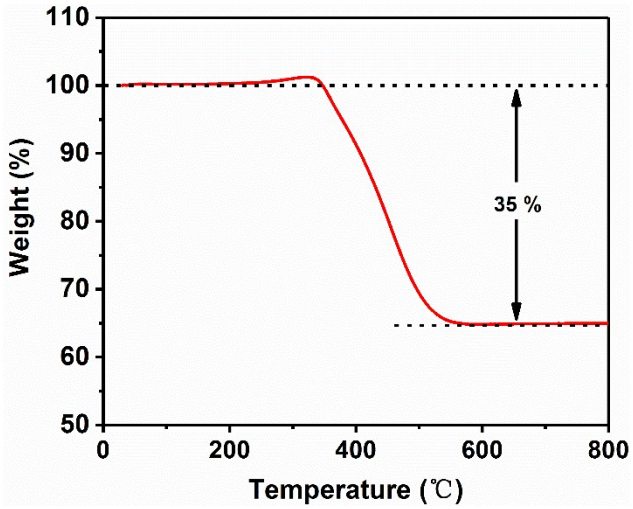

Fig. S4 TGA profile of Co-NCNTs under Air atmosphere from room temperature to 800 ˚C with a heating rate of 10 ˚C min^{-1}.

The content of Co in the Co-NCNTs is about 47.7 wt%, based on the TGA analysis. Since the solid product left after TGA only corresponds to Co_3O_4, the amount of Co present in the Co-NCNTs can be calculated using the following equation:

$$Co\ Content\ (\%) = n_1/n_2 * 73.4\% = 65\% * 73.4\% \approx 47.7\%$$

n_1 Represents the residual amount of the sample after TGA test;

n_2 Represents the initial amount of the sample before TGA test, where 73.4% is the mass fraction of Co atom in Co_3O_4.

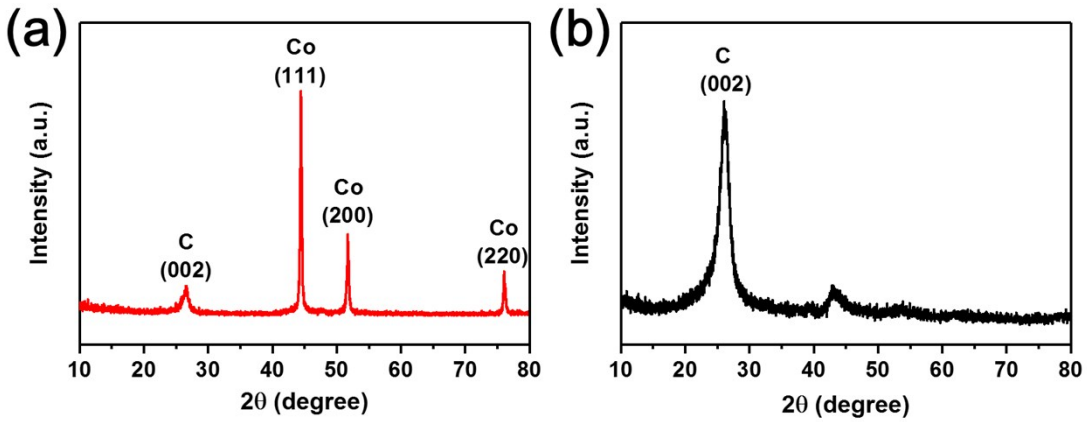

Fig. S5 XRD patterns of (a) Co-NCNTs and (b) commercial CNTs.

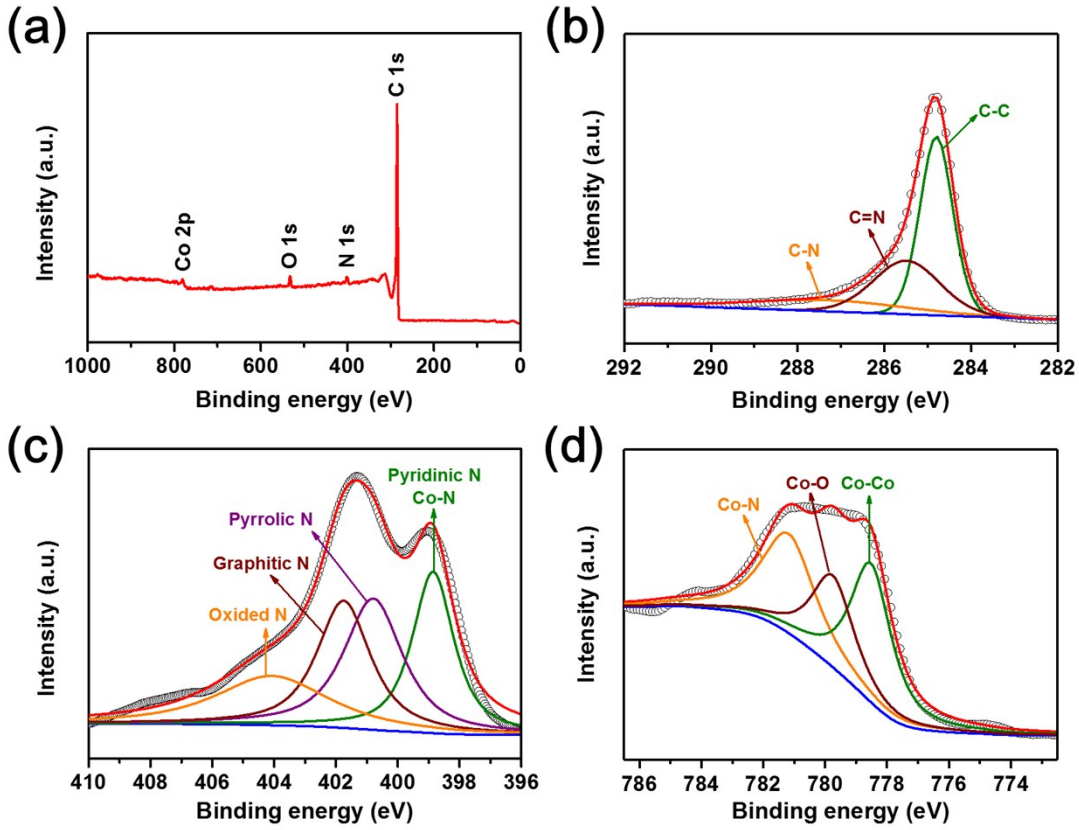

Fig. S6 XPS survey spectrum of Co-NCNTs. (a) full spectrum. (b) C1s. (c) N1s. (d) Co2p.

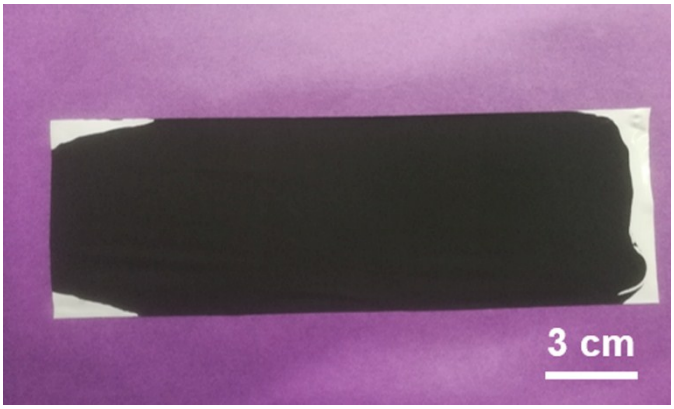

Fig. S7 Digital photographs of Co-NCNT coated separator prepared by blade coating method.

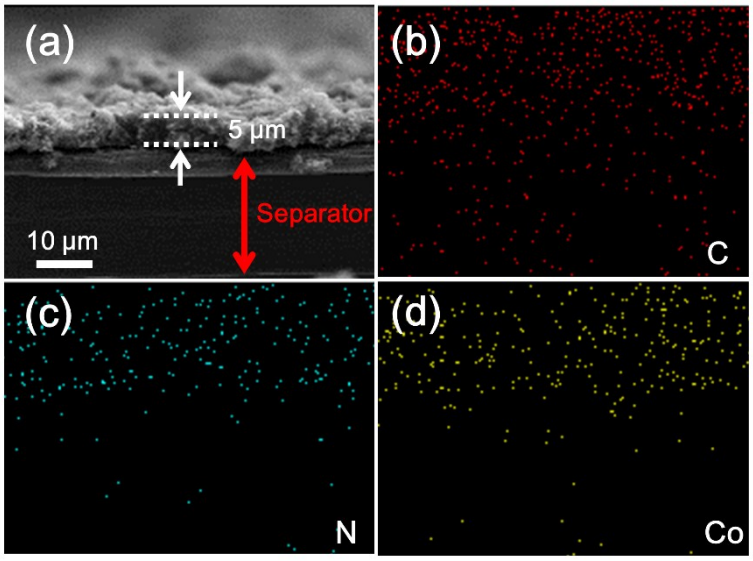

Fig. S8 (a) The cross-section SEM image of Co-NCNT coated separator and (b-d) corresponding EDS elemental mapping analysis.

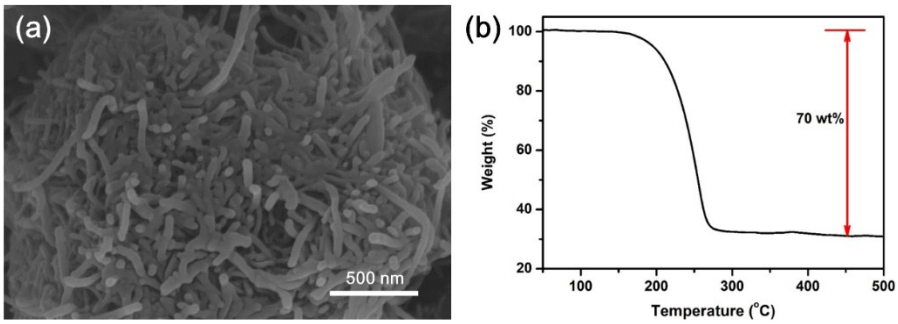

Fig. S9 (a) SEM image and (b) TGA curve of CNT/S composite.

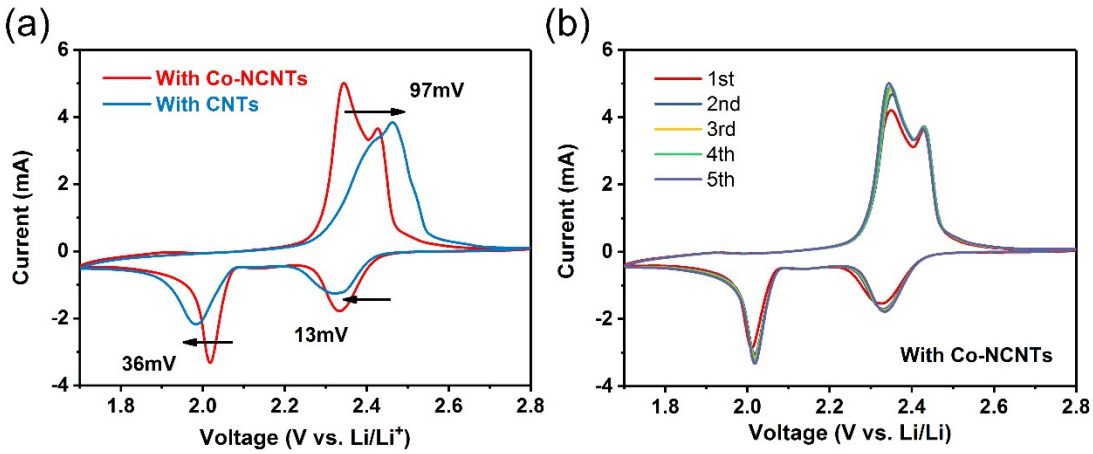

Fig. S10 (a) CV profiles of the Li–S batteries at a scan rate of 0.1 mV s^{-1} with Co-NCNT and CNT modified separator for the first cycle. (b) The CV profiles of the Li–S batteries at a scan rate of 0.1 mV s^{-1} with Co-NCNT modified separator for five cycles.

The cyclic voltammetry (CV) profiles of Li–S batteries with Co-NCNT and CNT modified separator are shown in Fig. S10a. The cells were measured in the voltage range 1.7–2.8 V at a scan rate of 0.1 mV s^{-1}. For the cell with a Co-NCNT modified separator, there were two distinct anodic and cathodic peaks in the CV curves, which is consistent with the typical electrochemical redox reaction of elemental sulfur. The first cathodic peak at 2.33 V corresponds to the phase transitions from solid sulfur to liquid high-order LiPSs (Li_2S_n, $4 \leqslant n \leqslant 8$). The second cathodic peak located at 2.02 V is ascribed to further reduction of liquid LiPSs to solid state Li_2S_2/Li_2S. The two anodic peaks are attributed to reverse conversion of solid Li_2S_2/Li_2S to liquid Li_2S_n and then back to sulfur. Notably, the Li–S cell with the CNT modified separator only showed one anodic peak and two cathodic peaks with much lower peak intensities compared with the Li–S cell based on Co-NCNT modified separator. In addition, the anodic peak positively shifted by about 97 mV, and the cathodic peaks negatively shifted by about 13 and 36 mV.

In the initial five cycles in Fig. S10b, there is no obvious change in both the CV peak positions and the peak currents, indicating the good stability of the cells with Co-NCNTs modified separators.

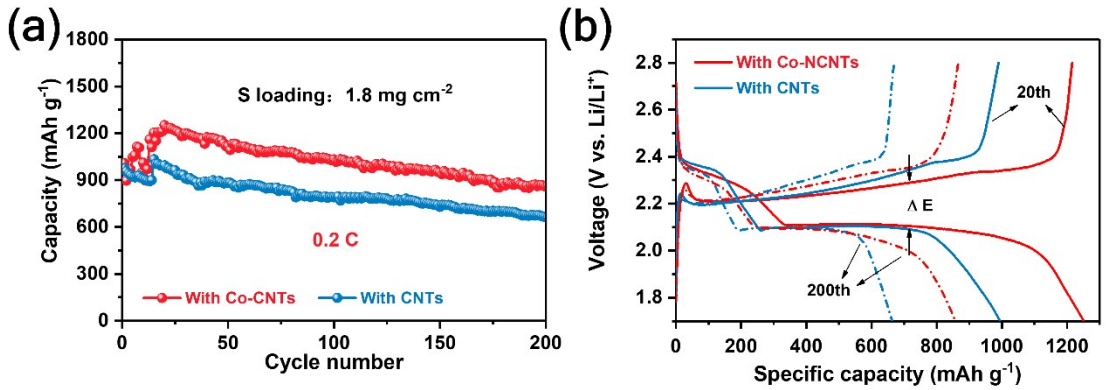

Fig. S11 Electrochemical performance of Li–S cells fabricated with Co-NCNT and CNT modified separator. (a) Cycling performances and coulombic efficiency at 0.2 C (sulfur loading: 1.8 mg cm^{-2}). (b) The 20th and 200th charge and discharge profiles at 0.2 C.

The galvanostatic charge and discharge profiles exhibited two characteristic discharge plateaus at about 2.32 and 2.1 V, respectively (Fig. S11b, ESI†), which is in agreement with the CV results. The 20th and 200th discharge capacities with the Co-NCNT modified separator were 1251.4 and 857.7 mA h g^{-1}, respectively, which were much higher than that with the CNT modified separator (994.2 and 663.5 mA h g^{-1}, respectively), suggesting better utilization of active materials. Moreover, the Li–S battery with the Co-NCNT modified separator showed decreased voltage hysteresis compared with that with the CNT modified separator, indicating faster redox kinetics and low resistance.

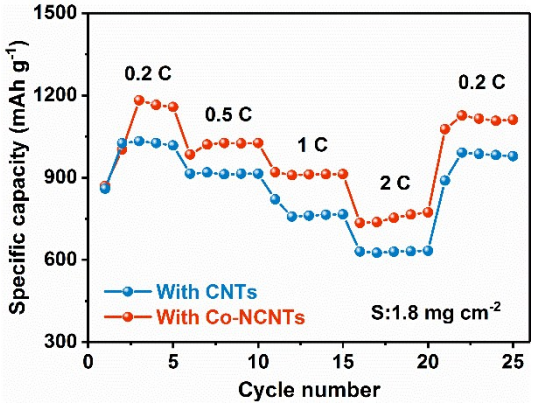

Fig. S12 Rate performance of Li-S batteries with Co-NCNTs and CNTs modified separator under various current rates (sulfur loading: 1.8 mg cm^{-2}).

The rate performance of the cell with the Co-NCNTs modified separator was significantly improved compared to that with the CNTs modified separator. The cell with the Co-NCNTs modified separator delivered a value of 1157.4 mA h g^{-1} at 0.2 C, and the reversible capacities decreased to 1026.1, 912.4 and 773.2 mA h g^{-1} at current rates of 0.5, 1 and 2 C, respectively. In comparison, the cells with the CNTs modified separator displayed inferior capacities of 914.1, 765.3 and 632.5 mA h g^{-1} at current rates of 0.5, 1 and 2 C, respectively. Finally, the capacity of cells with the Co-NCNTs modified separator recovered to 1076.3 mA h g^{-1} after current density decreased to 0.2C, while the CNTs modified separator showed a reversible capacities of 888.6 mA h g^{-1}.

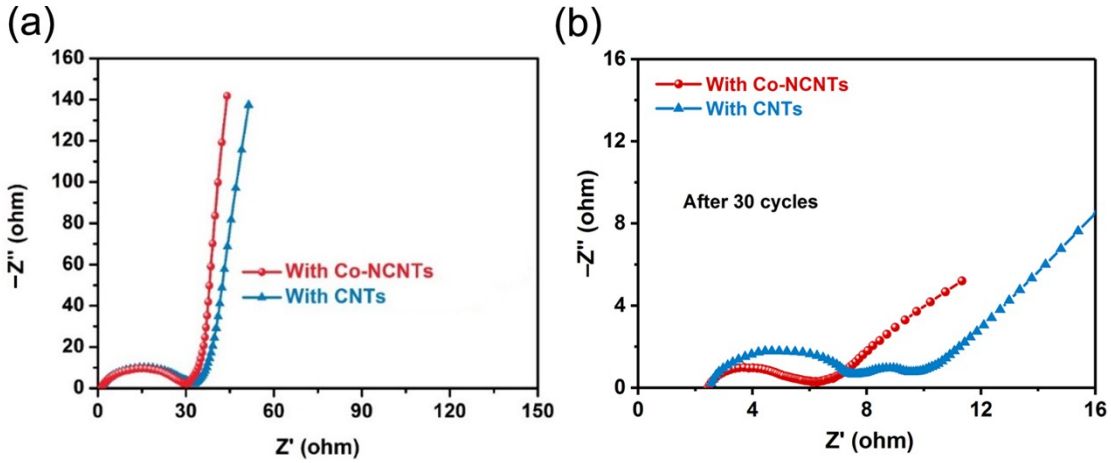

Fig. S13 EIS profiles of Li-S batteries with Co-NCNT and CNT modified separator (a) before and (b) after 30 cycles at 0.2 C.

AC impedance measurements of cells using different modified separators after 30 cycles at 0.2 C has been added in Fig. S13. After 30 cycling, the Rct value of Co-NCNTs was much smaller than that of CNTs, which could be attributed to the more uniform redistribution of the active sulfur in the Co-embedded conductive host during cycling.

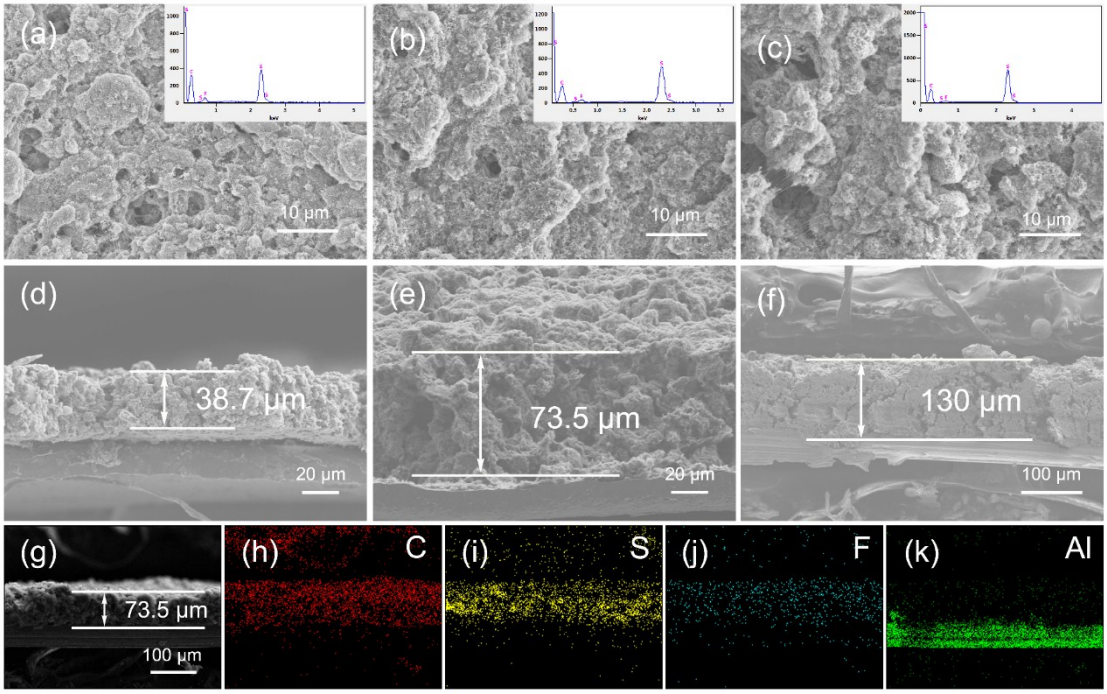

Fig. S14 the SEM images (a-c) and cross-section SEM images (d-f) of the CNT/S cathode with various sulfur loading amounts. (a, d) 1.8 mg cm^{-2}. (b, e) 2.7 mg cm^{-2}. (c, f) 4.3 mg cm^{-2}. Inset of (a-c) are corresponding EDS spectra image. (g-i) cross-section SEM image and corresponding EDS mapping images with a sulfur mass loading around 2.7 mg cm^{-2}.

The CNT/S cathode all exhibited a relatively flat surface with lots of macro-/meso-pores, which served as Li^+ channel for fast ion transportation. The cross-section SEM images showed that the thickness of the electrodes increase with sulfur loading amounts, which were 38.7, 73.5 and

130μm, respectively. EDS spectra showed the existence of carbon element, sulfur element and fluorine element in both samples. And cross-section SEM image and corresponding EDS mapping of the electrode also indicated the homogeneous distribution of C, S, F and Al.

Table S1 Summary of electrochemical performances of S/C cathodes using modified separators for Li–S batteries.

Modified separators (sample)	Mass loading on separator (mg cm^{-2})	Cathode Material (sulfur content)	Sulfur loading (mg cm^{-2})	Discharge rate	Cycle numbers	Discharge Capacity (mAh g^{-1})	Capacity decay rate per cycle	Ref.
Co-NCNTs coated separator	0.23	CNT-S (70%)	1.8	0.2 C	200	857.7	-	**This work**
			2.7	1 C	700	525.0	0.072%	
			4.3	0.1 C	100	867.4 (3.73 mA h cm^{-2})	-	
Nafion coated separator	0.7	CNT-S (50%)	0.53	1 C	500	780	0.08%	1
	3.5					781	0.082%	
Meso C Coated Separator	-	C–S composite (70%)	1.55	0.5 C	500	723	0.081%	2
				1 C		683	0.071%	
				2 C		591	0.062%	
PEDOT:PSS coated separator	0.07	Sulfur-expanded graphene composite	0.9-1.1	0.25 C	1000	626	0.0364%	3

		(80%)						
graphene@ carbon nanotubes coated separator	0.33	Activated Super P-Sulfur (75%)	1.4	0.2 1	200	935.1 755.6	-	4
MWCNT@ PEG modified separator	0.26	Acetylene black-Sulfur (60%)	1.6	1C	500	490	0.12%	5
$BaTiO_3$ coated separator	2.4	Ketjen black -S (60%)	5.0	0.1 C	50	929.5	-	6
Acetylene black-CoS_2 coated separator	0.5-0.7	AB-S Composite (77.8%)	1.5-2	2 C	450	380	0.09%	7
MWCNT /SPANI modified separator	0.4	C-PANI/S @PDA composite (90%)	5.0	0.0625 C (100 mA g–1)	100	913	-	8
N, P doped graphene coated separator	1.0-1.1	carbon black-sulfur (70%)	1.5	1 C	500	638	0.0898%	9
KB@Ir modified separator	0.2	KB/S composite (74.6%)	0.8 4.6	1 C 0.05 C	500 16	452 1148	0.105% -	10

Reference

1. J.-Q. Huang, Q. Zhang, H.-J. Peng, X.-Y. Liu, W.-Z. Qian and F. Wei, *Energy & Environmental Science*, 2014, **7**, 347-353.
2. J. Balach, T. Jaumann, M. Klose, S. Oswald, J. Eckert and L. Giebeler, *Adv. Funct. Mater.*, 2015, **25**, 5285-5291.
3. S. A. Abbas, M. A. Ibrahem, L.-H. Hu, C.-N. Lin, J. Fang, K. M. Boopathi, P.-C. Wang, L.-J. Li and C.-W. Chu, *J. Mater. Chem. A*, 2016, **4**, 9661-9669.
4. H. Wu, Y. Huang, W. Zhang, X. Sun, Y. Yang, L. Wang and M. Zong, *J. Alloys Compd.*, 2017, **708**, 743-750.
5. G. Wang, Y. Lai, Z. Zhang, J. Li and Z. Zhang, *J. Mater. Chem. A*, 2015, **3**, 7139-7144.
6. T. Yim, S. H. Han, N. H. Park, M.-S. Park, J. H. Lee, J. Shin, J. W. Choi, Y. Jung, Y. N. Jo, J.-S. Yu and K. J. Kim, *Adv. Funct. Mater.*, 2016, **26**, 7817-7823.
7. P. Zeng, L. Huang, X. Zhang, Y. Han and Y. Chen, *Appl. Surf. Sci.*, 2018, **427**, 242-252.
8. L. Shi, F. Zeng, X. Cheng, K. H. Lam, W. Wang, A. Wang, Z. Jin, F. Wu and Y. Yang, *Chem. Eng. J.*, 2018, **334**, 305-312.
9. X. Gu, C.-j. Tong, C. Lai, J. Qiu, X. Huang, W. Yang, B. Wen, L.-m. Liu, Y. Hou and S. Zhang, *J. Mater. Chem. A*, 2015, **3**, 16670-16678.
10. P. Zuo, J. Hua, M. He, H. Zhang, Z. Qian, Y. Ma, C. Du, X. Cheng, Y. Gao and G. Yin, *J. Mater. Chem. A*, 2017, **5**, 10936-10945.